Non-coding RNA Research 10 (2025) 140–152

Contents lists available at ScienceDirect

Non-coding RNA Research

journal homepage: www.keaipublishing.com/en/journals/non-coding-rna-research

Original Research Article

Upregulation of circGDI2 inhibits tumorigenesis by stabilizing the expression of RNA m6A demethylase FTO in oral squamous cell carcinoma

Yuwei Gu [a,b], Ling Sheng [a], Xiaoxiao Wei [c], Yuling Chen [a], Yuntao Lin [a], Zhangfu Li [a], Xiaolian Li [a], Huijun Yang [a], Yufan Wang [a], Hongyu Yang [a,b,c,*], Yuehong Shen [a,b,c,**]

[a] Department of Oral and Maxillofacial Surgery, Stomatological Center, Peking University Shenzhen Hospital, Guangdong Provincial High-level Clinical Key Specialty, Guangdong Province Engineering Research Center of Oral Disease Diagnosis and Treatment, The Institute of Stomatology, Shenzhen Peking University the Hong Kong University of Science and Technology Medical Center, Guangdong, 518036, China
[b] Department of Oral and Maxillofacial Surgery, Peking University School and Hospital of Stomatology, Beijing, 100081, China
[c] Peking University Shenzhen Hospital Clinical College, the Fifth School of Clinical Medicine, Anhui Medical University, Hefei, Anhui, 230032, China

ARTICLE INFO

Keywords:
CircGDI2
Oral squamous cell carcinoma
CircRNAs
FTO

ABSTRACT

Background: Oral squamous cell carcinoma (OSCC) is a malignant tumour that is difficult to identify and prone to metastasis and invasion. Circular RNAs (circRNAs) are important cancer regulators and can be used as potential biomarkers. However, OSCC-related circRNAs need to be further explored. We investigated the role of circGDI2 in OSCC and explored its downstream regulatory mechanisms.

Methods: Quantitative real-time PCR was used to detect the expression levels of circGDI2 and fat mass and obesity-associated protein (FTO) in cells. Lentiviral transfection was used to construct stable circGDI2 overexpressing cells for subsequent cell function tests. RNA pull-down, RNA Immunoprecipitation (RIP), western blotting, and protein stability assays were conducted to detect circGDI2 binding proteins and their functions. CCK8, Transwell, and wound healing assays were used to verify cell functions after overexpressing circGDI2 or suppressing FTO expression. Animal experiments were performed to verify the results *in vivo*.

Results: The expression of circGDI2 was markedly decreased in both OSCC cell lines and patient tissues. Overexpression of circGDI2 in OSCC cell lines led to decreased proliferation, migration, and invasion abilities. Knockdown of circGDI2 showed the opposite trend. CircGDI2 has been validated to interact with the FTO protein within cells, as evidenced by mass spectrometry and RIP assays. This interaction was found to prevent the degradation of the FTO protein. Dot blot analysis showed a reduction in N6-methyladenosine (m6A) modification after circGDI2 overexpression. Reduced FTO levels reversed the inhibitory effects of circGDI2 overexpression on cell proliferation, migration, and invasion *in vitro* and on tumorigenesis *in vivo*.

Conclusions: CircGDI2 functions as a tumour suppressor by binding to the FTO protein to reduce RNA m6A modification levels and ultimately inhibit proliferation and migration in OSCC cells. This study indicates the potential use of circGDI2 as a new target for the prevention and treatment of OSCC.

1. Background

Oral cancer is the sixth most prevalent cancer worldwide, with approximately 377,713 new cases and nearly 177,757 deaths reported globally in 2020 [1]. Oral squamous cell carcinoma (OSCC) accounts for over 90 % of all oral cancers and is the most prevalent malignant tumour of the lips and mouth. Due to the intricate nature of early detection and the abundance of blood vessels and nerves in the head and neck, some patients are diagnosed in the later stages of the disease, often with the presence of metastases. Although treatment methods have been improved in recent years, the mortality rate in Asia is as high as 73.3 % [2], and the overall survival rate of OSCC is not optimal; therefore, identifying new biomarkers is essential for the early detection and treatment of OSCC.

* Corresponding authors. Department of Oral and Maxillofacial Surgery, Stomatological Center, Peking University Shenzhen Hospital, 1120 Lianhua Road, Futian, Shenzhen, Guangdong, 518036, China.
** Corresponding author. Department of Oral and Maxillofacial Surgery, Stomatological Center, Peking University Shenzhen Hospital, 1120 Lianhua Road, Futian, Shenzhen, Guangdong, 518036, China.
E-mail addresses: hyyang192@hotmail.com (H. Yang), yuehongshen@hotmail.com (Y. Shen).

https://doi.org/10.1016/j.ncrna.2024.08.001
Received 10 May 2024; Received in revised form 9 July 2024; Accepted 8 August 2024
Available online 9 August 2024

Circular RNAs (circRNAs) are non-coding RNAs with closed circular structures. Most are derived from the reverse splicing of exons in the protein-coding gene precursor messenger RNA (mRNA) [3]. Owing to the absence of a 5′ cap end and a 3′ poly (A) tail in their ring structure, circRNAs can avoid degradation and are stably expressed in intracellular or extracellular vesicles and body fluids. Tissue-specific expression and excellent detectability make circRNAs potential biomarkers for physiological and pathological processes [4–7], such as in different types of cancers. Many studies have shown that dysregulated circRNAs can promote or inhibit tumour progression [5]. For instance, hsa_circ_0050386 has been reported to inhibit the development of non-small cell lung cancer [8], while circSTX6 promotes tumorigenesis in pancreatic ductal carcinoma, bladder cancer, and hepatocellular carcinoma [9–11]. CircRNAs are involved in several aspects of OSCC onset and progression [12]. For instance, circKRT1 promotes the invasion and migration of OSCC cells and is closely related to the tumour microenvironment [13]. CircANKS1B mediates cisplatin resistance via miRNA sponging [14]. However, the specific mechanisms and roles of newly identified circRNAs require further elucidation.

N6-methyladenosine (m6A) has been widely studied as the most abundant intracellular modification in cancers [15]. The modifying enzymes, “writer”, “eraser”, and “reader”, affect the transcription, translation, splicing, and other processes of target RNA by changing the m6A modification level, which exerts dual roles in tumorigenesis [16]. Fat mass and obesity-associated protein (FTO) was the first discovered m6A demethylase, which binds to the m6A modification site of the RNA molecule and exerts a demethylation effect [17,18]. FTO is highly expressed in most tumors and plays a significant role in promoting cancer. However, it also functions as a tumour suppressor in certain cancers, such as clear cell renal cell carcinoma [19] and bladder cancer [20]. Studies on FTO were predominantly focused on downstream regulatory pathways, including AKT phosphorylation, RNA stabilization, and activation of STAT3 signaling [21]. However, the molecular mechanism responsible for the alteration in FTO expression remains unclear.

A newly identified circRNA derived from GDP dissociation inhibitor 2 (GDI2) is expressed at low levels in OSCC and has not yet been thoroughly investigated in OSCC development. Our study demonstrated that circGDI2 is downregulated in OSCC, suppressing proliferation, migration, and invasion of OSCC cells and reducing cellular m6A modification levels by enhancing FTO stability. Reduced FTO levels reversed the inhibitory effects of circGDI2 overexpression on cell proliferation, migration, and invasion *in vitro* and on tumorigenesis *in vivo*. CircGDI2 may be a novel marker for the early diagnosis and treatment of OSCC.

2. Methods

2.1. Clinical tissue samples

Forty tumour tissues and adjacent normal tissues were obtained from patients with OSCC at the Department of Oral and Maxillofacial Surgery, Peking University Shenzhen Hospital. All excised specimens were promptly preserved at −80 °C. This study was approved by the Ethics Committee of Peking University Shenzhen Hospital (No. 2022–117). All patients provided written informed consent.

2.2. Cell culture

Human oral keratinocytes (HOKs) used in this study were purchased from the Chinese Academy of Sciences (Shanghai, China). OSCC cell lines (SCC15 and CAL27) were purchased from the American Type Culture Collection (ATCC, VA, USA). All cell lines were cultured in a humidified incubator at 37 °C and 5 % CO_2, using Dulbecco’s modified Eagle’s medium (DMEM; Gibco, CA, USA) supplemented with 10 % foetal bovine serum (FBS; Gibco) and 1 % penicillin/streptomycin (Pricella, Wuhan, China).

2.3. RNA extraction and quantitative real-time PCR (qRT-PCR)

Total RNA was isolated from OSCC tissues and cells using TRIzol Reagent (Takara, Japan). First-strand cDNA was synthesized from the RNA samples, and quantitative PCR was performed using the SYBR Green Premix Kit (Accurate Biology, Hunan, China) on a LightCycler 480 (Roche, Switzerland). Target gene expression was analyzed using the $2^{-\Delta\Delta Ct}$ method, normalized to β-actin or GAPDH.

Primer sequence.

circGDI2,
Forward: 5′-GCCCATACCTTTATCCACTC-3′,
Reverse: 5′-GTCAACATTCCAGTCTCTTCCT-3′,
FTO,
Forward: 5′-TTGCCCGAACATTACCTGCT-3′,
Reverse: 5′-TGTGAGGTCAAACGGCAGAG-3′;
β-actin,
Forward: 5′-AAACTGGAACGGTGAAGGTG-3′,
Reverse: 5′-AGTGGGGTGGCTTTTAGGAT-3′.
GAPDH,
Forward:5′-GGAGCGAGATCCCTCCAAAAT -3′,
Reverse: 5′-GGCTGTTGTCATACTTCTCATGG-3′.

2.4. Sanger sequencing

cDNA was generated from 500 ng of total RNA using the PrimeScript RT Master Mix (Takara, Japan) to identify circGDI2. PCR was performed to amplify circGDI2 with divergent primers targeting the distal ends of circRNA from the cDNA templates using PrimeSTAR HS DNA Polymerase (Takara, Japan). DNA products were verified using Sanger sequencing (Sangon, Shanghai, China).

2.5. RNase R treatment

Total RNA (5 μg) was incubated at 37 °C for 10 min with or without 5 U of RNase R (GENESEED, Guangzhou, China). Subsequently, the PrimeScript RT Master Mix (Takara, Japan) was used to reverse transcribe 1 μg of the RNA into cDNA.

2.6. RNA subcellular distribution assay

The Nuclear and Cytoplasmic Extraction Reagents (Thermo Fisher Scientific, USA) were used to extract nuclear and cytoplasmic fractions. RNA was then extracted and reverse transcribed into cDNA. The circGDI2 levels in fractions were examined using qRT-PCR.

2.7. Fluorescence in situ hybridization (FISH) assay

The circGDI2 bioprobe, synthesized by Sangon Biotech (Shanghai, China), was used in this study. The probe signal was detected using an in situ hybridization kit (GENESEED, China), in accordance with the methods reported previously [22]. Samples were fixed with paraformaldehyde and pre-treated using the kit. The probes were then diluted 200-fold with hybridization buffer and denatured at 85 °C for 3 min, followed by hybridization at 37 °C for 24 h. After washing and blocking, the cells were incubated with biotin antibody (Rhodamine--Conjugate) for 1 h, and the nuclei were counter-stained with DAPI in an antifade solution. Samples were observed using STELLARIS5 microscope (Lecia, Germany).

circGDI2 bioprobe:
Sense: agaactgccccaaggatttgcaaggaatgtatcctgtcaggtataatg
Antisense: cattatacctgacaggatacattccttgcaaatccttggggcagttct

2.8. Cell transfection

A lentiviral overexpression plasmid containing GFP and the puromycin-resistant gene was constructed by HanBio Co., Ltd. (Shanghai, China). The cells were inoculated in 24-well plates and cultured until reached 30–50 % confluency. Subsequently, medium containing the lentiviral vector was added and incubated for 48 h. The medium was replaced with a 5 μg/mL puromycin hydrochloride-containing medium to screen for infected cells. After incubation for two weeks, stable cells were selected and cultured in medium containing 0.5 μg/mL puromycin. The overexpression efficiency of circGDI2 was verified using qRT-PCR.

For FTO and circGDI2 knockdown, small interfering RNA (siRNA) targeting FTO (siFTO: 5′-GACAAAGCCTAACCTACTT-3′), circGDI2 (si-circGDI2: 5′- GATTTGCAAGGAATGTATCCTTT-3) and control siRNA were purchased from Hanbio (Shanghai, China). Cells were cultured in 6-well plates. Once the cell reached 50 % confluency, siRNA transfection was conducted using Lipofectamine 3000 following the manufacturer's guidelines.

2.9. CCK8 assay

Stable cells were seeded at a density of 5×10^3 cells/well in 96-well plates. After incubation for the specified time (0, 24, 48, and 72 h), cells were incubated with 10 μL CCK-8 reagent (Aboro, Guangdong, China) for 1 h. Absorbance was measured at 450 nm using Multiskan GO (Thermo Fisher, USA).

2.10. Wound-healing assay

OSCC cells were seeded in 6-well plates. The cells were scratched with the tip of a 200 μL pipette, when the cells reached 100 % confluency. The detached cells were removed by Phosphate Buffered Saline (PBS) washing. All cells used in the wound-healing experiments were cultured in DMEM with 1 % FBS. The area of each scratch was assessed under a microscope at specific time points.

2.11. Transwell migration and invasion assays

For the migration assay, stable cell lines cultured in serum-free media were seeded into the upper chambers, and DMEM supplemented with 10 % FBS was added to the bottom chambers. After 24 or 48 h of culture, the cells were immobilized using 4 % paraformaldehyde solution and treated with 0.05 % crystal violet dye for 30 min. Subsequently, images were captured under microscope (Olympus, Tokyo, Japan), and cell counts were obtained. The conditions for the invasion assay were similar to those used for the migration assay except Matrigel (Coning, Shanghai, China) was added to the upper chambers before cell seeding.

2.12. RNA pull-down assays

After routine transfection of CAL27 cells, approximately 1×10^7 cells were washed with PBS buffer three times, lysed with 500 μL pre-cooled Radio Immunoprecipitation Assay Lysis (RIPA) buffer, and treated with 3 g biotinylated DNA oligonucleotide probe targeting the endogenous or exogenous expression of circGDI2 at room temperature for 2 h. Approximately 50 μL of streptavidin magnetic beads were added to each binding reaction and incubated at room temperature for 2 h, then washed briefly 4 times with wash buffer. Binding proteins in the pull-down materials were analyzed using 4–12 % FuturePAGE (ACE, Jiangsu, China).

2.13. Mass spectrometry

CircGDI2 pull-down samples were analyzed using mass spectrometry (ShenZhen SMQ Group Medical Laboratory, Shenzhen, China). Proteins in the samples were extracted, enzymatically digested, and the resulting peptides enriched and separated. The peptides were identified through high-performance liquid chromatography coupled with tandem high-resolution mass spectrometry, generating extensive mass spectrum data. The Human UniProt library (https://www. Uniprot. org/) was used for protein identification. The identified proteins were further subjected to bioinformatic analysis.

2.14. m6A dot blot

Total RNA, diluted to 800 ng/μL, was mixed with an equal volume of RNA denaturing solution (20 × SSC buffer: 37 % deionised formaldehyde = 3:2) and denatured at 95 °C for 5 min. A 2 μL mixture was rapidly spotted onto a nitrocellulose transfer member (GE HealthCare, UK) and cross-linked at 120 °C in an oven for 30 min. Membrane was blocked with 2 % BSA Albumin Fraction V (BioFroxx, Germany) for 2 h and hybridized overnight with m6A monoclonal antibody (cat # ABE572, Millipore, Darmstadt, Germany) at 4 °C. The following day, the HRP-conjugated anti-rabbit immunoglobulin G (Beyotime, Shanghai, China) was incubated with the membrane for 1 h before luminescence was measured. Membrane was then stained with blue methylene solution (Solario, Beijing, China) to visualise the loaded RNA.

2.15. RNA immunoprecipitation (RIP)

RIP was performed using a Magna RIP kit (Millipore, Germany). CAL27 cells were lysed in the RIP buffer. Magnetic beads conjugated with immunoglobulin G antibodies (IgG, cat. # PP64B, Millipore, Germany) or FTO monoclonal antibodies (Proteintech, USA) were used to isolate protein-bound RNA from cell lysates, respectively. FTO binding efficiency was determined by western blotting. The eluate was purified, and the expression level of circGDI2 was quantified using qRT-PCR.

2.16. Protein stability assays

The SCC15 control and overexpression groups were seeded onto 3.5 cm dishes. Protein biosynthesis was inhibited using 10 μM Cycloheximide (CHX, HY-12320, MCE, USA) when the cell confluency was 90 %. In the meanwhile, 15 μM MG-132 (HY-13259, MCE, USA) was added to the control group to inhibit protein degradation. Samples were collected at 0, 4, 8, and 12 h after drug treatment. The extracts were analyzed by western blotting to verify the expression levels of the target proteins.

2.17. Western blot assays

The lysates from tissues and cells were obtained using RIPA buffer. After 100 °C denaturation, the lysates were electrophoresed using sodium dodecyl sulfate-polyacrylamide gel electrophoresis (SDS-PAGE). The proteins were transferred onto polyvinylidene fluoride (PVDF) membranes (Millipore, Ireland), blocked with 5 % nonfat milk for 1.5 h, washed with TBST, and incubated with primary antibodies overnight (anti-FTO, 1:2000 Proteintech; anti-β-actin, 1:2000 Bioss; anti-GAPDH, 1:2000 Bioss). The following day, the membrane was incubated with horseradish peroxidase-conjugated antibodies for 1 h and exposed to electrochemiluminescent (ECL) luminescent liquid (Biosharp, Anhui, China).

2.18. Establishment of mouse xenograft models

BALB/c nude mice aged 5 weeks (Yaokang, Gongdong, China) were randomly divided into two groups and injected subcutaneously with 100 μL of cell suspension containing 2×10^6 SCC15-circGDI2 cells and SCC15-control cells, respectively. Tumour growth was monitored every 3 days, and mice were sacrificed after 30 days of observation.

For the rescue experiment, 10 nude mice were subcutaneously

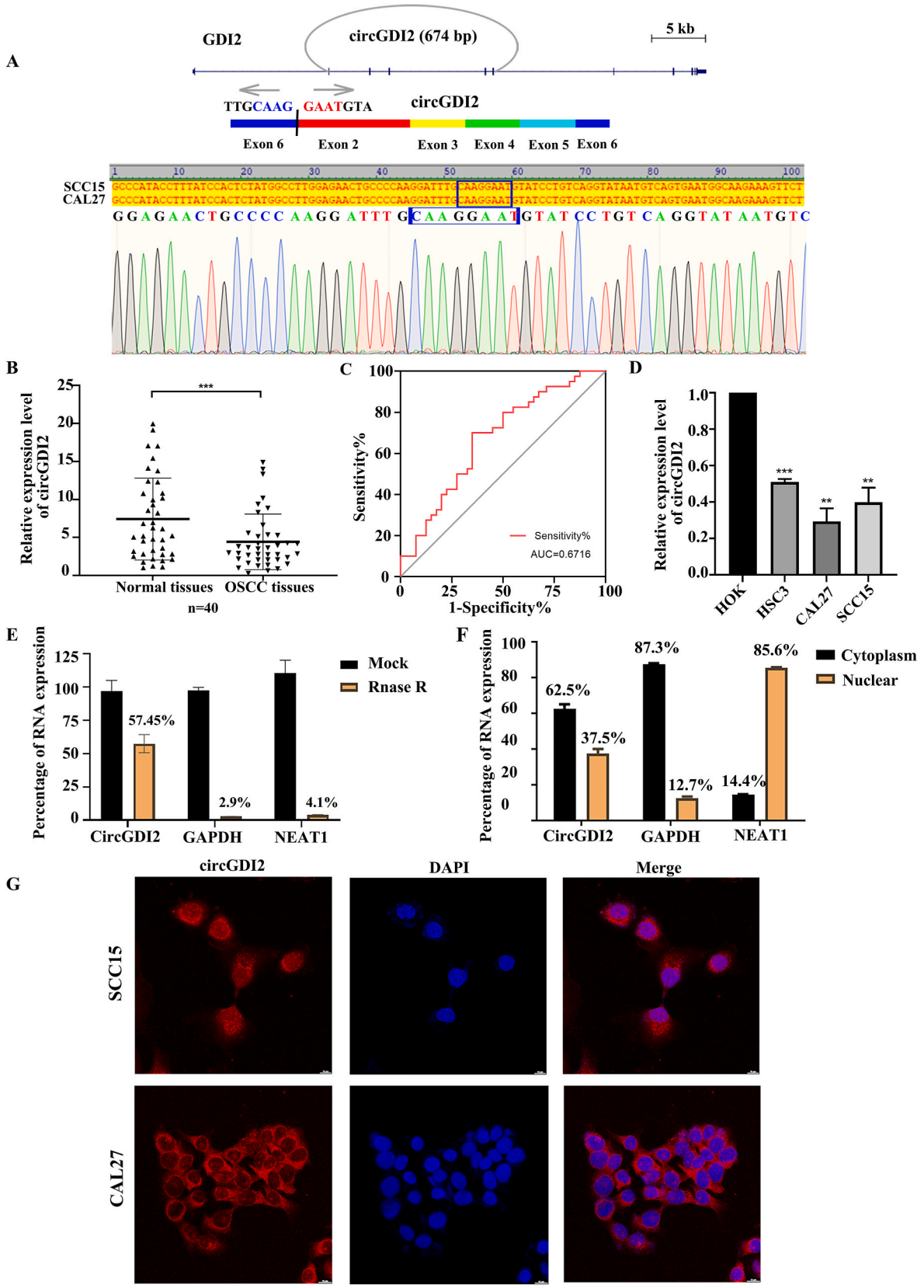

Fig. 1. Characterisation of circGDI2 in OSCC. (A) Schematic representation of the genomic locus of circGDI2 derived from exon 2 to exon 6 of GDI2. The expression of circGDI2 was confirmed through Sanger sequencing in SCC15 and CAL27 cells. The blue frame represents the junction region between exon 6 and exon 2. (B) Relative expression of circGDI2 was determined in tissues from 40 OSCC patients. (C) The diagnostic value of circGDI2 in OSCC patients was assessed via ROC curve analysis. (D) Expression of circGDI2 in OSCC cell lines (HSC3, CAL27, and SCC15) and normal HOK cell lines was determined using qRT-PCR analysis. (E) qRT-PCR was used to detect the abundance of circGDI2 in CAL27 cells treated with RNase R. (F) The percentage of circGDI2 in the cytoplasm and nucleus was assessed by qRT-PCR. Data were presented as means ± S.D., $^{**}p < 0.01$, $^{***}p < 0.001$. (G) The subcellular localization of circGDI2 was observed by FISH assay. Scale bars, 10 μm.

Table 1
Association between the expression of circGDI2 and clinicopathological characteristics in 40 patients with OSCC.

Feature	No. Of patients	circGDI2 Expression, Median (IQR)	*P* value
Gender			0.5420
Male	26	12.88 (12.23–13.73)	
Female	14	13.27 (12.70–13.73)	
Age			0.1250
< 60	26	12.82 (12.23–13.58)	
≥60	14	13.34 (12.99–14.23)	
Differentiation grade			0.0078[a]
Well	20	12.60 (11.56–13.32)	
Moderate-Poor	20	13.41 (12.75–14.27)	
Lymph node status			0.1219
Negative	19	12.84 (11.62–13.66)	
Positive	21	13.25 (12.69–14.03)	
TNM stage			0.2570
I-II	11	12.84 (11.42–13.73)	
III-IV	29	13.23 (12.55–13.73)	

Mann-Whitney test.
[a] $p < 0.01$.

injected with SCC15-circGDI2 cells. Two weeks after xenograft implantation, mice were randomly divided into two groups: (1) injected with siNC and (2) injected with siFTO. The siRNAs were modified by 5′Chol +2′OMe modification strategy. (5 nmol; RiboBio, Guangzhou, China). Treatment was administered every 3 days for two weeks. Tumour volume was measured every 3 days and calculated as length × width^2 × 0.5. Tumors were dissected for Immunohistochemistry (IHC) staining. The following antibodies were used: anti-FTO (1:1000, Proteintech), anti-ki67 (1:3200, CST).

2.19. Statistical analysis

The data analysis was performed using Image J and GraphPad Prism (v9.0). Data were presented as mean ± SEM or SD, which were obtained from three independent experiments. Group differences were conducted using Student's *t*-test or Mann–Whitney test, with $p < 0.05$ considered statistically significant.

3. Results

3.1. Characteristics of circGDI2 in OSCC

According to CircBank data, circGDI2 is derived from exons 2 to 6 of the GDI2 gene, which is reverse-spliced to form a 674 bp-sized circRNA. Identification of circGDI2 was confirmed using Sanger-sequencing in the CAL27 and SCC15 cell lines (Fig. 1A). To verify the expression levels of circGDI2 in OSCC tissues, we performed qRT-PCR analysis on 40 pairs of OSCC and adjacent normal tissues after surgery. The circGDI2 expression level was decreased in OSCC tissues compared to that in normal tissues (Fig. 1B). Analysis of the clinicopathological features of these 40 patients indicated a significant correlation between circGDI2 expression and OSCC differentiation grade (Table 1). Receiver operating characteristic (ROC) curve analysis yielded an area under the curve of approximately 0.6716, a sensitivity of 70 %, and a specificity of 65 %, which suggested circGDI2 is diagnostically meaningful for OSCC (Fig. 1C). Moreover, we verified the circGDI2 expression levels in HOK and OSCC cell lines (CAL27, HSC3, and SCC15), demonstrating significant downregulation of circGDI2 in OSCC cells compared to HOK cells (Fig. 1D). As control, mRNAs of *gapdh* and nuclear paraspeckle assembly transcript 1 (*neat 1*) were liner and abundantly expressed in the cytoplasm and nucleus, respectively. RNase R exonuclease digestion was performed to investigate the stability of circGDI2 in OSCC cells. Compared to linear RNAs, circGDI2 maintained RNase R exonuclease resistance (Fig. 1E). The intracellular localization of circRNAs usually plays a functional role in biological processes. Using qRT-PCR to detect circGDI2 levels in the nucleus and cytoplasm, we found that 62.5 % of circGDI2 was present in the cytoplasm (Fig. 1F). These results were supported by FISH experiments, which indicated that circGDI2 was mainly enriched in the cytoplasm of CAL27 and SCC15 cell lines. (Fig. 1G). In summary, circGDI2 is a stable circRNA that is significantly down-regulated in OSCC tissues and cell lines.

3.2. CircGDI2 inhibits the migration, proliferation, and invasion of OSCC

To explore the role of circGDI2 in OSCC occurrence and development, we examined the proliferation, migration, and invasion of OSCC cells. Plasmids encoding the circGDI2 construct were expressed in CAL27 and SCC15 cells by lentiviral infection. Using puromycin selection, stable circGDI2 overexpression cell lines were obtained. Quantified by qRT-PCR, the expression level of circGDI2 in the overexpressed cells was more than 15-fold higher than that in the control group (Fig. 2A). To explore the effect of circGDI2 on the proliferation of OSCC cells, we seeded OSCC cells in 96-well plates and added CCK8 reagent to detect the absorbance at 0, 24, 48, and 72 h (Fig. 2B). The results showed that circGDI2 overexpression decreased the proliferative ability of OSCC cells (Fig. 2B). The migration ability of tumors was assessed through wound-healing and Transwell migration experiments (Fig. 2C and D). The results showed that the circGDI2 overexpression group had a wider gap remaining compared to the control group. The wound-healing rate was significantly decreased in the circGDI2 overexpression group (Fig. 2C). Similarly, the Transwell migration experiments revealed decreased migration of cells from the upper to lower chamber in the circGDI2 overexpression group compared with the control group (Fig. 2D). Both experiments indicated that circGDI2 overexpression inhibits OSCC cell migration. Matrigel was applied to the Transwell chamber to investigate tumour cell invasion. After 48 h of incubation, the circGDI2 overexpression group had fewer invasive cells than the control group, suggesting reduced invasion (Fig. 2E). Xenograft assays were performed to determine the role of circGDI2 in tumourigenesis *in vivo*. Tumour growth was slower in the group injected with circGDI2 overexpression cells compared to the control group (Fig. 3A). Cells overexpressing circGDI2 showed lower tumour weights and volumes (Fig. 3B and C). Collectively, these findings indicate that circGDI2 inhibited the proliferation, migration, invasion, and tumourigenesis of OSCC cells.

In the meanwhile, we assessed the impact of circGDI2 knockdown on OSCC cell lines (CAL27 and SCC15) using siRNAs. The knockdown efficiency was confirmed via qRT-PCR (Supplementary Fig. 1A). The knockdown group showed increased proliferation (Supplementary Fig. 1B), enhanced wound-healing (Supplementary Fig. 1C), and elevated migration (24 h) and invasion (48 h) as measured by Transwell assays (Supplementary Figs. 1D and E). These results indicate that the suppression of circGDI2 enhances the proliferative, migratory, and invasive properties of OSCC cells.

3.3. CircGDI2 binds to demethylase FTO and affects the m6A methylation level

To explore the possible downstream regulation of circGDI2, we conducted RNA pull-down experiments. The circGDI2 probe was designed to attract circGDI2-bound proteins in cell lysates. The binding proteins were applied to silver staining and identified using mass spectrometry (Fig. 4A). The results were compared with the UniProt database. GO enrichment analysis showed that circGDI2-bound proteins were mainly enriched in biological processes, particularly RNA splicing and translation. Notably, most of these proteins were RNA-binding proteins with RNA-binding domains, indicating their involvement in RNA post-transcriptional modifications (Fig. 4B–E). Overall, 65.7 % of circGDI2-bound proteins were RNA-binding proteins, including six m6A methylation-related enzymes (FTO, IGF2BP3, UGF2BP2, YTHDF1,

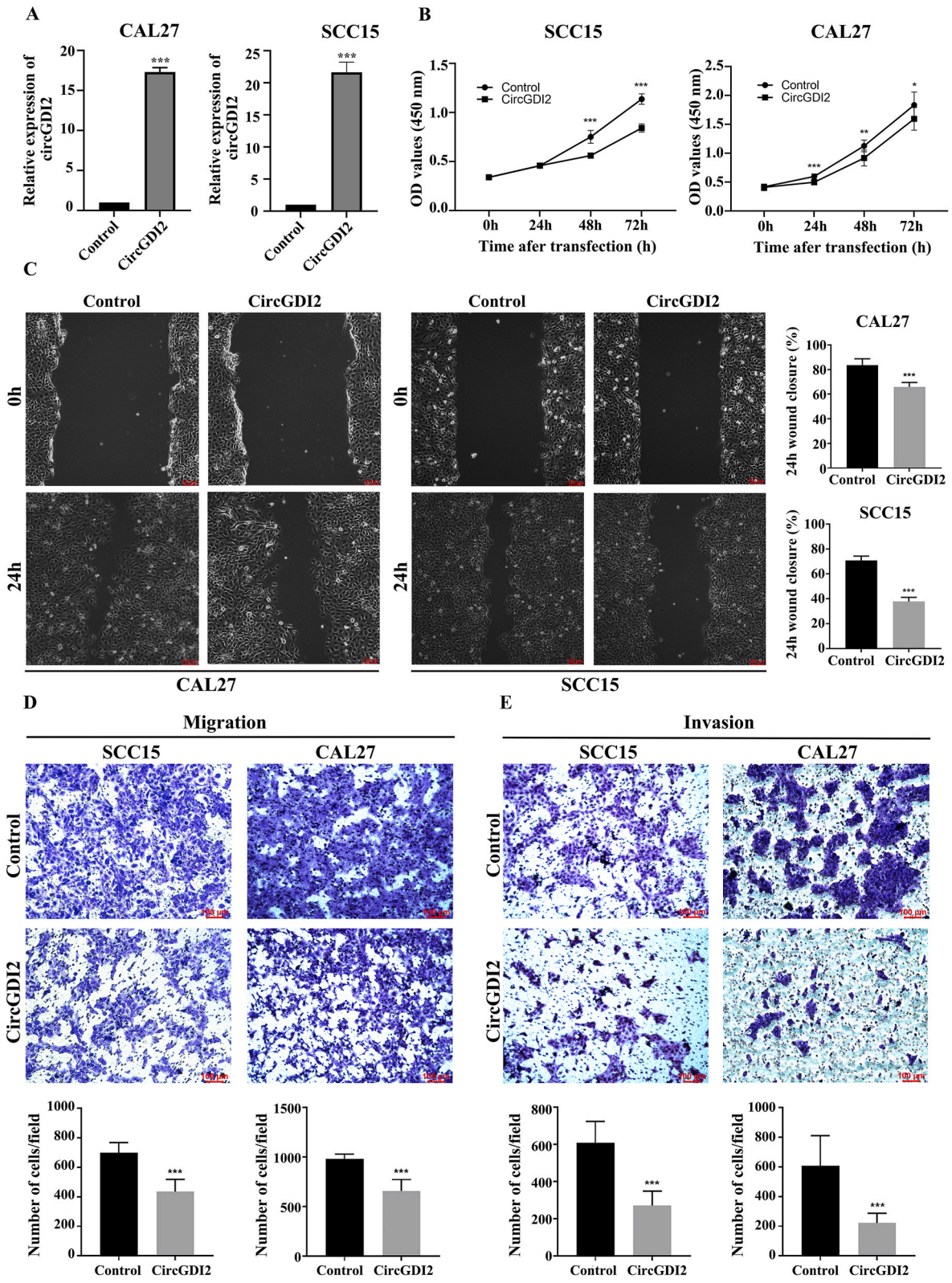

Fig. 2. Overexpression of circGDI2 inhibits proliferation, migration, and invasion of OSCC cells. (A) CAL27 and SCC15 cell lines were infected with a recombinant lentivirus harboring circGDI2 expression vector (circGDI2) or negative-control vector (control). The circGDI2 expression was determined using qRT-PCR. (B) The proliferation ability of stable OSCC cells was assessed using CCK8 assays. (C) Wound-healing assays were conducted, and the wound closure ratios at 24 h were quantified. (D, E) The Transwell migration (D) and invasion (E) assays were performed using SCC15 and CAL27 stable cells. The number of migrated or invaded cells per field was quantified, and the data were presented as means ± SD, *p < 0.05, **p < 0.01, ***p < 0.001, Scale bars, 100 μm.

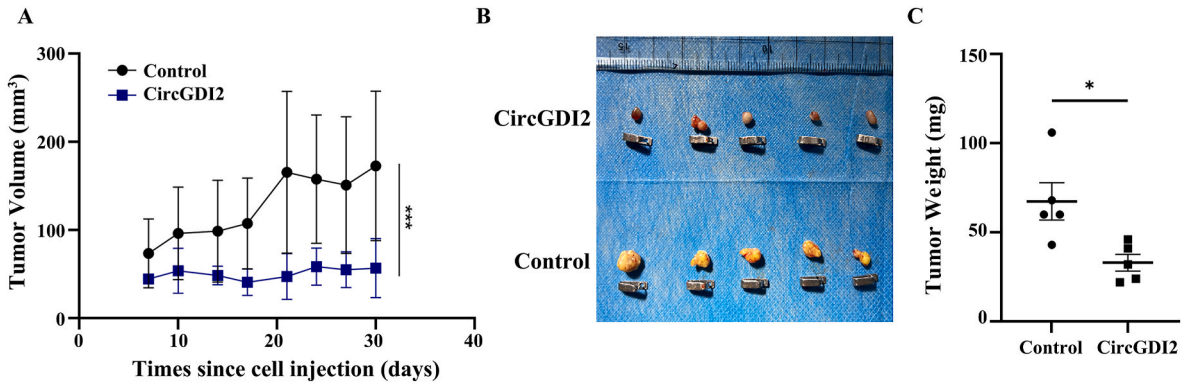

Fig. 3. Overexpression of circGDI2 inhibits the tumorigenesis of OSCC *in vivo*. The SCC15 stable cells overexpressing circGDI2 or negative control were injected into nude mice, respectively. (A) The tumour volumes were recorded every 3 days. (B) The image of tumors. (C) The tumour weight of each group. Data were presented as means ± SD, *p < 0.05, ***p < 0.001.

YTHDF2, and YTHDF3) (Fig. 4F). To further investigate the regulatory role of circGDI2, m6A dot blotting was performed, revealing that CAL27 and SCC15 cells exhibited increased m6A methylation levels compared to normal HOK cells, whereas circGDI2 overexpression decreased m6A methylation levels in OSCC cells (Fig. 4G). Given that FTO is a methyltransferase among the six m6A methylation-related enzymes, it may play a downstream role in regulating circGDI2-mediated methylation.

Western blotting verified that the FTO protein (58 kD) was enriched in the circGDI2 probe group (Fig. 5A), proving that circGDI2 and FTO exhibited specific binding. RIP further confirmed this binding in OSCC cells. When FTO was pulled down by FTO antibodies in OSCC cell lysates, western blotting results showed that FTO was specifically immunoprecipitated (Fig. 5B). The qRT-PCR verification showed that circGDI2 expression in the FTO pull-down group increased up to 52 fold compared to the control group (Fig. 5C). These results affirmed the interaction between FTO and circGDI2 in OSCC cells. To evaluate the impact of the interaction between circGDI2 and FTO, we examined the expression of FTO mRNA in the circGDI2 overexpression and control groups. The findings revealed no significant difference of FTO mRNA expression levels both in the CAL27 and SCC15 cell lines (Fig. 5D). However, western blotting experiments demonstrated the increase of FTO protein level in the circGDI2 overexpression group than that in the control group (Fig. 5E). We conducted protein stability assays to examine whether the circGDI2-FTO interaction affects protein stability. Cycloheximide (CHX) is a commonly used protein synthesis inhibitor by inhibiting mRNA translation [23]. With CHX treatment, FTO was significantly degraded in the control group at 8 h, while degradation was less obvious in the circGDI2 overexpression group even at 12 h after treatment (Fig. 5F). MG-132 is a proteasome inhibitor commonly used to inhibit protein degradation [24]. By adding MG-132, protein degradation was significantly inhibited in the control group (Fig. 5F). These results suggested that circGDI2 binds to FTO and increases its stability, consequently reducing m6A methylation levels in OSCC cells.

3.4. FTO knockdown reverses the effect of circGDI2 on the OSCC

To investigate whether FTO knockdown reversed the inhibitory effects of circGDI2 overexpression on OSCC, siRNA transient transfection was performed in both control and circGDI2 groups. The knockdown efficiency was approximately 60 %, as determined by western blotting and qRT-PCR (Fig. 6A). In the CCK8 assay, circGDI2 overexpression decreased cell viability compared with controls, whereas FTO knockdown restored cell proliferation rates in the circGDI2 overexpression group (Fig. 6B). Wound-healing experiments showed that circGDI2 overexpression at 24 h reduced the closure rate, whereas FTO knockdown rescued the wound-healing rate by approximately 20 % at 24 h in both the SCC15 and CAL27 cell lines (Fig. 6C). Transwell migration experiments were performed to verify the migratory ability of CAL27 and SCC15 cells. After 24 h of incubation, the number of migrated cells in the overexpression circGDI2 group was significantly reduced, whereas FTO knockdown rescued the migrated cells significantly (Fig. 6D). Similarly, in Transwell invasion assays, the invasive cells in circGDI2-overexpressing group decreased compared to that in the control group, while FTO knockdown enhanced OSCC cell invasion (Fig. 6E). In summary, the data indicated that the reduction of FTO expression counteracts the effects of circGDI2 overexpression on the viability, migration, and invasiveness of OSCC cells. The rescue experiments were also performed *in vivo*. Two weeks after the injection of SCC15-circGDI2 cells, we established an OSCC model in BALB/c nude mice. The mice were randomly divided into two groups. After siRNA injection, the growth rate in the siFTO group was higher than that in the siNC group (Fig. 7A). Tumour weight and volume in the siFTO group were significantly higher than those in the siNC group (Fig. 7B and C). The siFTO group exhibited a diminished level of FTO protein, confirming the efficacy of the siRNA-mediated knockdown. Additionally, this group displayed elevated Ki67 expression, indicative of enhanced tumour proliferation relative to the siNC group (Fig. 7D). These *in vivo* experiments confirmed that FTO knockdown reversed the tumorigenic effects of circGDI2. Overall, these findings demonstrated that FTO knockdown rescues the inhibitory effect of OSCC invasion, migration, and proliferation caused by circGDI2 overexpression in OSCC, suggesting that FTO may be a downstream regulator of circGDI2.

4. Discussion

OSCC is the most prevalent form of oral cancer, characterized by malignancy in the oral mucosal epithelium. The incidence of the disease has increased rapidly in both developing and developed countries in recent decades [25]. The high mortality rate of OSCC is due the difficulty in early detection [26]. Early-stage OSCC usually does not present lymph node metastasis, thus offering a favourable postoperative survival rate. Therefore, increasing the screening and detection rates of OSCC and achieving early diagnosis and treatment are important to improve the prognosis and minimize recurrence in patients with OSCC [26,27].

In recent times, circRNAs have been extensively investigated as potential markers for early cancer detection. The development of high-throughput sequencing has led to more newly identified circRNAs in OSCC, and more than 120 circRNAs have been extensively studied in the past five years [12]. Most studies have shown that circRNAs are involved in OSCC development and are potential biomarkers and therapeutic targets [28–31]. For instance, circGDI2 was mentioned in the transcriptome analysis of diabetic nephropathy [32] and is predicted to be a key molecule in the competing endogenous RNAs network of neuroblastoma [33]. However, this has not been investigated thoroughly in

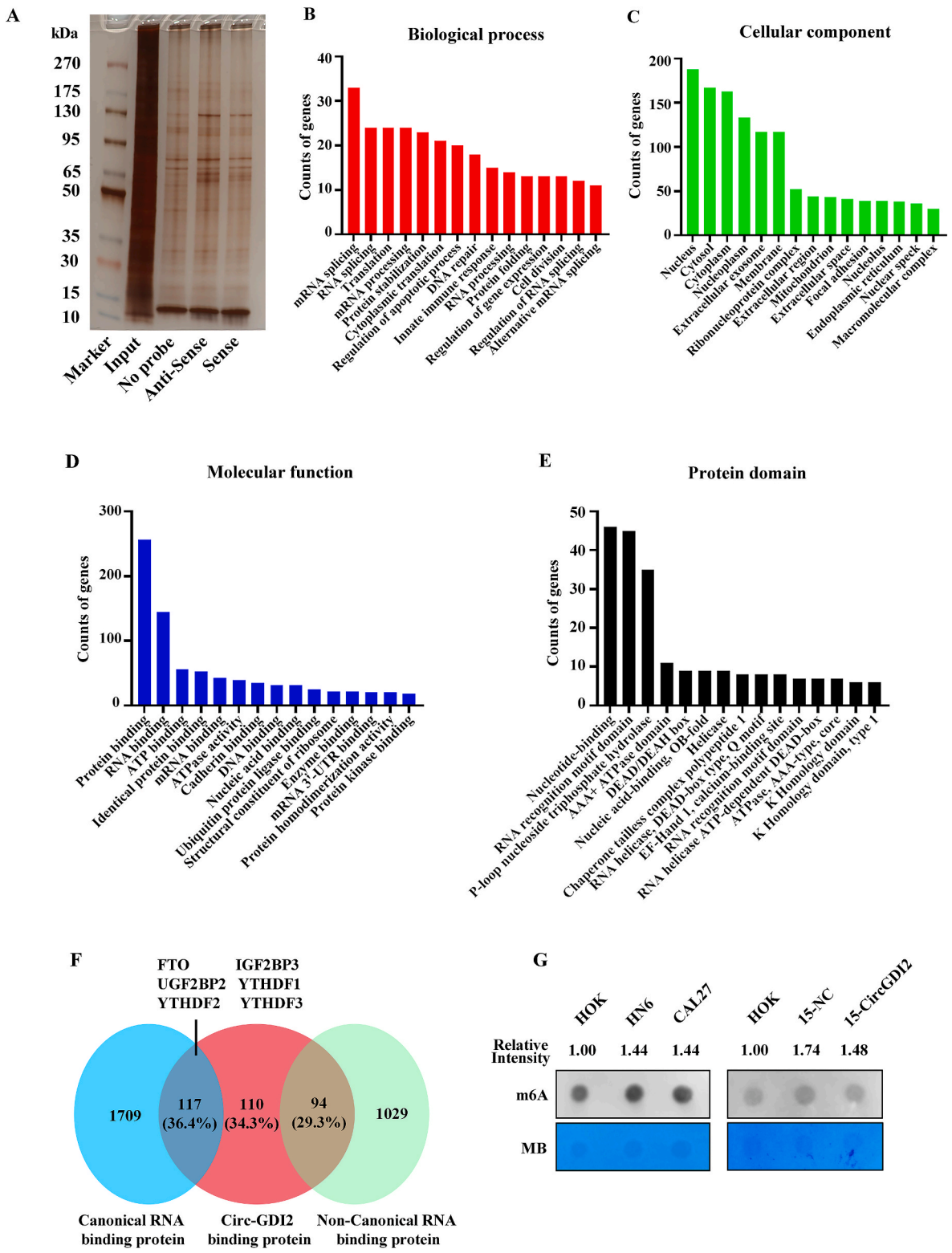

Fig. 4. CircGDI2 associated proteins affect the m6A methylation. (A) The circGDI2 probe pull-down of bound protein eluate was detected using silver staining and analyzed by mass spectrometry. (B–E) GO enrichment and protein domain analysis were performed. (F) Venn diagram showing canonical RNA binding proteins, circGDI2 binding proteins, and non-canonical RNA binding proteins. (G) Methylation levels were detected using a dot blot in HOK, HN6, CAL27 cells, and stable SCC15 cells expressing circGDI2 or the control vector.

patients with OSCC. In this study, low expression of circGDI2 was demonstrated in OSCC tissues and cell lines. It was correlated with the differentiation grades of OSCC, indicating that circGDI2 could be a potential diagnostic marker for early OSCC screening. In addition, by constructing circGDI2 overexpression cell lines, we designed cell experiments to confirm that circGDI2 inhibits the proliferation, migration, and invasion of OSCC cells.

In addition to being stable biomarkers, circRNAs also play significant

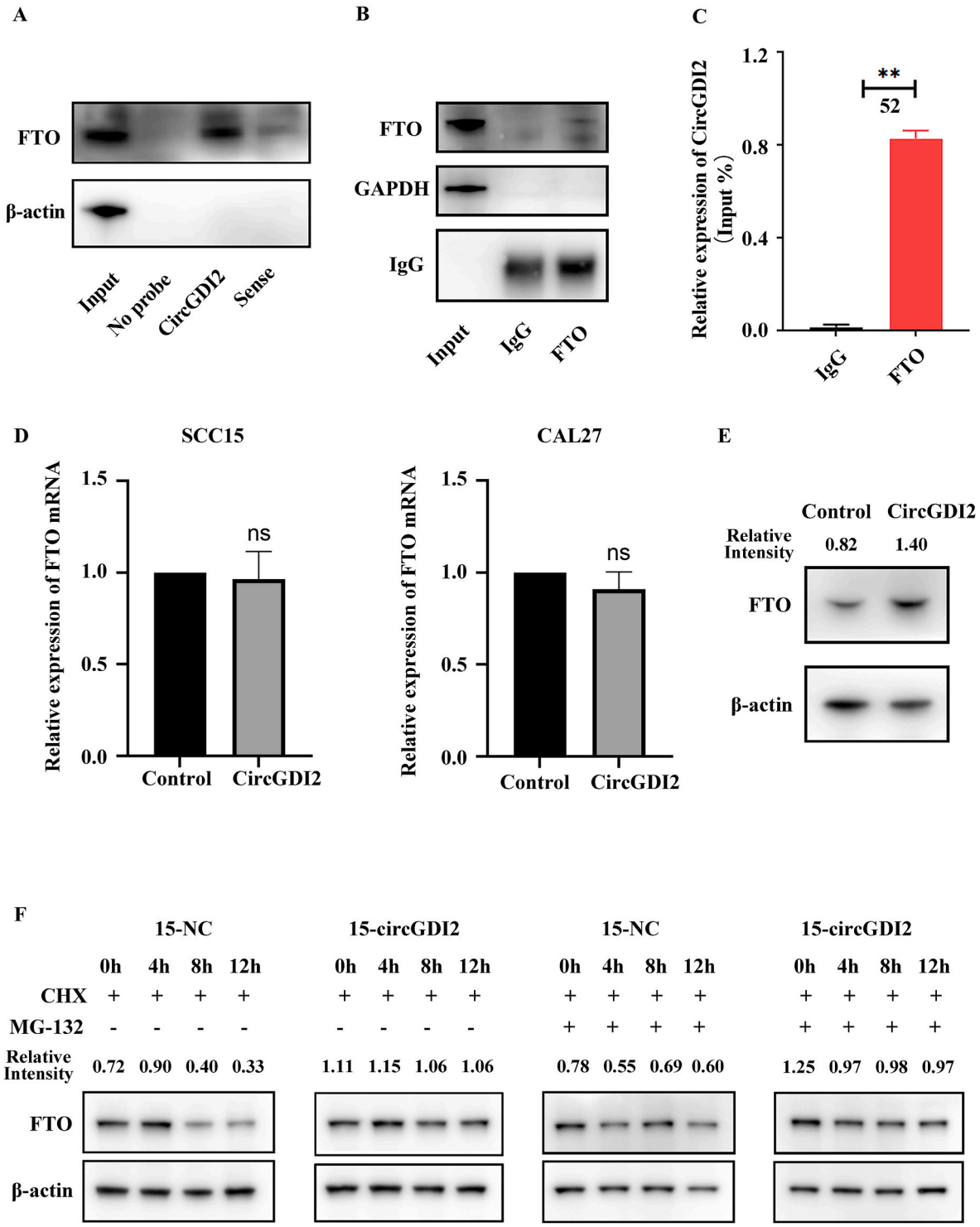

Fig. 5. CircGDI2 interacts with FTO. (A) Immunoprecipitation was conducted using probes targeting circGDI2 in CAL27 cells. The precipitates were analyzed using specified antibodies. (B) FTO immunoprecipitation was performed. (C) The enrichment of circGDI2 in FTO immunoprecipitation were examined using qRT-PCR. (D) qRT-PCR was used to verify the FTO mRNA expression level in the control group and the circGDI2 overexpression group. (E) Western blot analysis was used to verify the expression of FTO in the control group and the circGDI2 overexpression group in SCC15 cells. (F) Western blot analysis was used to verify FTO stability. SCC15 cells in the control group and circGDI2 overexpression group were treated with 10 μM CHX alone or 10 μM CHX and 15 μM MG-132, for 0, 4, 8, and 12 h, respectively.

biological roles [34]. They can sponge mRNAs, encode proteins, mediate mRNA translation, and interact with RNA-binding proteins (RBPs). In recent years, an increasing number of studies have demonstrated the crosstalk between circRNAs and m6A [35]. Most studies focused on m6A regulatory influence on circRNA production, transport, and biological function by changing the stability and binding to pre-mRNA [36–38]. Further research is needed to explore how circRNAs modulate m6A methylation by affecting the activity of related enzymes [35]. Our findings indicate that circGDI2 binds to m6A methylation-related enzymes and reduces the overall m6A methylation levels in OSCC cells,

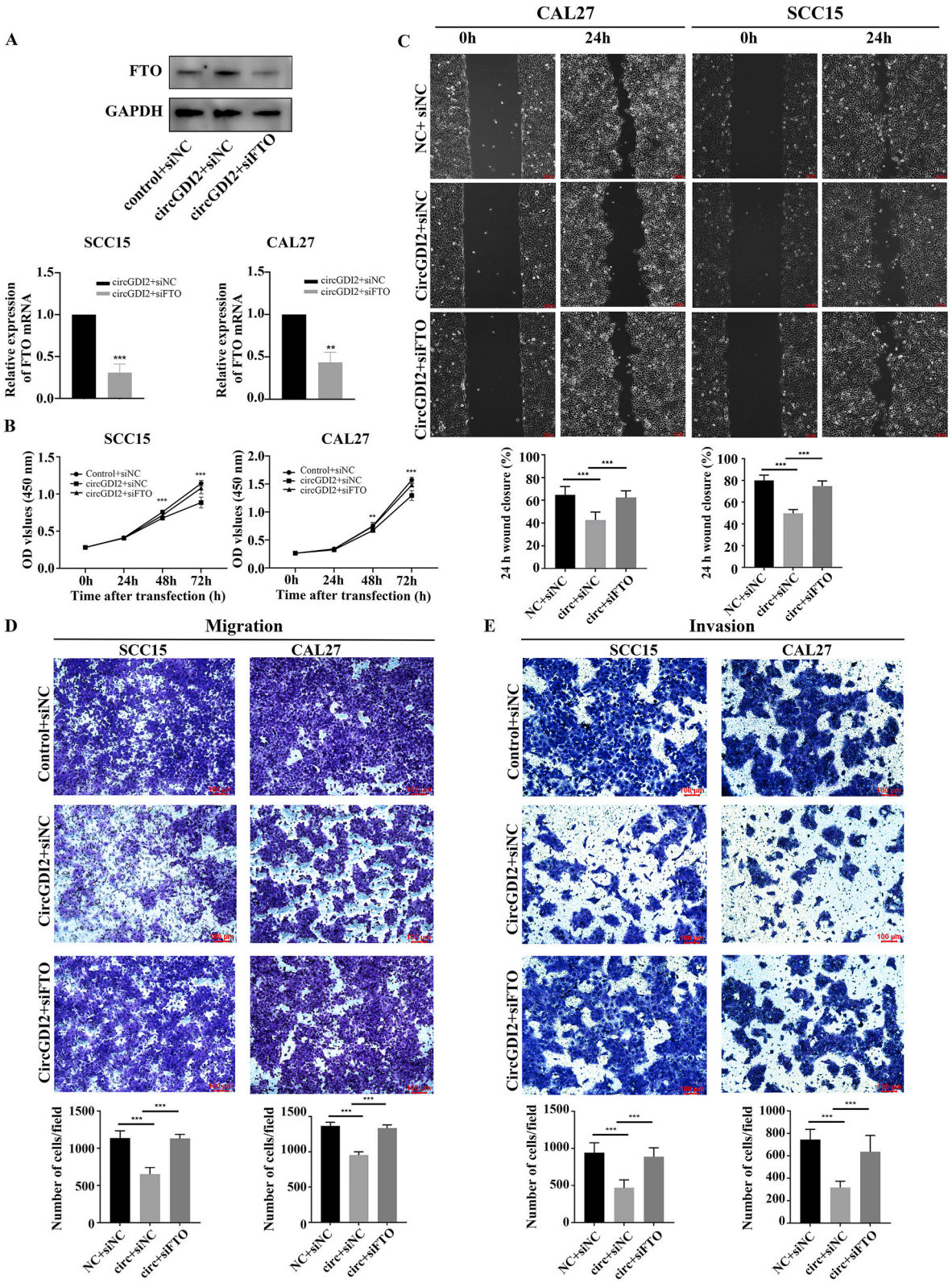

Fig. 6. Knockdown of FTO reverses the inhibition of circGDI2 on proliferation, migration, and invasion of OSCC cells. (A) Western blot analysis and qRT-PCR were used to determine the knockdown efficiency of siFTO. (B) CCK8 assay was used to detect the effect of siFTO on stable cell viability. (C) A wound-healing assay was conducted to evaluate the effect of siFTO on cell migration. (D, E) The Transwell migration (D) and invasion assays (E) were performed and the number of migrated and invaded cells was quantified. Data were presented as means ± SD, $^{**}p < 0.01$, $^{***}p < 0.001$. Scale bars, 100 μm.

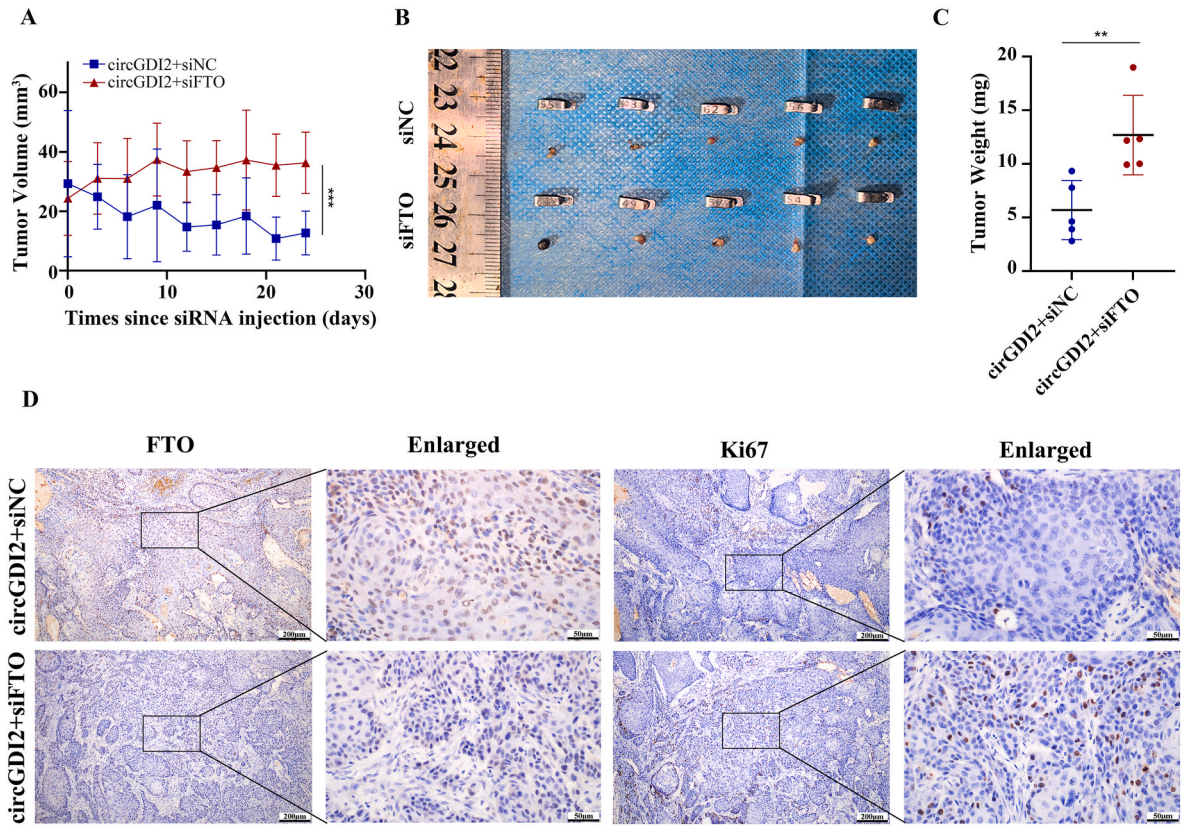

Fig. 7. Knockdown of FTO reverses the inhibition of circGDI2 on the tumorigenesis *in vivo*. The SCC15 stable cells overexpressing circGDI2 were injected into nude mice for two weeks to generate OSCC tumour. OSCC tumour-bearing nude mice were injected with siNC or siFTO. (A) After siRNA injection, the tumour volume was recorded every 3 days for 24 days. (B) The dissection of solid tumors. (C) Quantification of tumour weight. (D) IHC staining of FTO and Ki67 in the two groups. Data are presented as means ± SD, $^{**}p < 0.01$, $^{***}p < 0.001$.

suggesting the possibility of circGDI2 regulating m6A levels via binding to RBP in OSCC. Notably, RIP results confirmed that the demethylase FTO is bound to circGDI2 in cells. As a classic m6A demethylase, FTO plays a dual role in tumors. In the field of OSCC, studies on FTO have focused on the relationship between FTO expression and downstream regulatory mechanisms. Wang et al. showed that FTO exerts OSCC-promoting effects by altering the methylation level of eIF4G1 [39]. Li et al. highlighted the role of FTO in regulating YAP1 mRNA stability, which is relevant to OSCC progression [40]. Li et al. confirmed that the FTO/MYC/PD L1 signaling pathway plays a key role in promoting the malignant progression of OSCC [41]. Despite these insights, it is necessary to study the upstream regulation and monitor FTO protein levels. Our research revealed that circGDI2 modulates an upregulation of FTO protein expression. CircRNAs can influence stability of mRNA and proteins. RNA stability assays are typically employed to examine the decay rate of specific mRNA transcripts [42,43]. In our investigation, however, qRT-PCR data indicated that the elevated intracellular levels of FTO protein following circGDI2 overexpression were not a result of augmented mRNA transcription. Consequently, employing CHX to inhibit protein synthesis, we uncovered that the interaction with circGDI2 augmented the stability of the FTO protein, thereby promoting demethylation activity within the cells.

Studies have indicated that the proteasomal pathway is responsible for the degradation of FTO, with the K216R residue serving as a pivotal target for ubiquitin-dependent proteolysis [44]. In colorectal cancer, the FTO K216R loci in combination with STRAP E3 ubiquitin ligase mediated degradation [45]. In our research, the application of the proteasome inhibitor MG-132 mitigated the degradation of the FTO protein, thereby confirming that proteasome-mediated mechanisms contribute to FTO turnover in OSCC. We hypothesized that the interaction between circGDI2 and FTO could stabilize FTO by modulating its ubiquitination site, thereby affecting its degradation. The specific molecular underpinnings and structural alterations induced by the circGDI2-FTO interaction necessitate additional investigation.

To explore the involvement of FTO in circGDI2 regulation in OSCC, we designed rescue experiments. We demonstrated that knockdown FTO reverses the tumour inhibition effect in circGDI2 overexpressed cell lines. The results were validated *in vivo* by local injection of siRNA into solid tumors to determine the role of FTO as a downstream regulator of circGDI2. These results showed that circGDI2 binding to FTO reduced cellular m6A levels and inhibited OSCC development. Literature has indicated that FTO may attenuate the Wnt signaling pathway, thereby suppressing epithelial–mesenchymal transition process [46], or influence the stability of anti-cancer or pro-cancer genes through mRNA demethylation [21]. These findings may provide insights for further exploration of circGDI2/FTO/m6A demethylation pathways.

In OSCC, circRNA research has mainly been focused on sponging miRNAs, with mechanistic research primarily focusing on proliferation- and migration-related pathways [47]. The studies on m6A methylation are limited, with a focus primarily on circRNA self-methylation; for example, m6A-modified circFOXK2 promotes metabolic changes in OSCC [48]. And high-throughput analysis of m6A-modified circRNA in OSCC [12]. This study is novel in examining the relationship between circRNA and m6A methylation-related enzymes in OSCC tumorigenesis. This study enriches the research of circRNA in OSCC and lays a foundation for further exploration of the relationship between m6A levels and circRNA. However, this study has certain limitations. The specific binding site of circGDI2 and FTO was not identified, and there is a lack of in-depth studies on the specific mechanism of how circGDI2 affects FTO stability. In addition to m6A level changes, the downstream regulatory

mechanism of circGDI2 binding to FTO needs to be further explored.

5. Conclusion

Our study found that circGDI2 was significantly associated with the progression of OSCC, revealing the importance of the circGDI2-FTO-m6A signaling axis in OSCC. CircGDI2 directly binds to the FTO protein to achieve m6A demethylation, inhibiting the proliferation, invasion, and migration of OSCC cells. This study provides a new potential biomarker and effective therapeutic target for the treatment and prognosis of OSCC.

Ethics approval and consent to participate

This study was approved by the Ethics Committee of Peking University Shenzhen Hospital (No. 2022–117). All patients provided written informed consent. Animal experiments were approved by Shenzhen PKU-HKUST Medical Center (2023–1301) and conducted in strict compliance with animal ethics.

Consent for publication

Not applicable.

Availability of data and materials

All data generated or analyzed in the current study are available from the corresponding author on reasonable request.

Competing interests

All researchers declare declared no competing interests.

Funding

This work was supported by the Basic Research Program of the Shenzhen Innovation Council (JCYJ20200109140208058 and SGDX20210823103200005), Shenzhen High-level Hospital Construction Fund, Peking University Shenzhen Hospital Scientific Research Fund (KYQD2023253), Shenzhen Clinical Research Center for Oral Diseases (20,210,617,170,745,001), the Sanming Project of Medicine in Shenzhen (SZSM 202111012, Oral and Maxillofacial Surgery Team, Professor Yu Guangyan, Peking University Hospital of Stomatology) and Shenzhen Fund for Guangdong Provincial High-level Clinical Key Specialties (No. SZGSP008).

CRediT authorship contribution statement

Yuwei Gu: Writing – review & editing, Writing – original draft, Validation, Software, Methodology, Investigation, Formal analysis, Data curation. **Ling Sheng:** Validation, Software, Resources, Formal analysis, Data curation. **Xiaoxiao Wei:** Software, Methodology, Investigation, Formal analysis, Data curation. **Yuling Chen:** Writing – original draft, Data curation. **Yuntao Lin:** Data curation. **Zhangfu Li:** Methodology, Formal analysis, Data curation. **Xiaolian Li:** Data curation. **Huijun Yang:** Data curation. **Yufan Wang:** Data curation. **Hongyu Yang:** Writing – review & editing, Visualization, Project administration, Methodology, Funding acquisition, Formal analysis, Data curation. **Yuehong Shen:** Writing – review & editing, Visualization, Validation, Resources, Project administration, Methodology, Conceptualization.

Declaration of competing interest

The authors declare that they have no known competing financial interests or personal relationships that could have appeared to influence the work reported in this paper.

All researchers declare declared no competing interests.

Acknowledgements

We acknowledge the support from ShenZhen SMQ Group Medical Laboratory for protein mass spectrometry detection.

List of abbreviations

(OSCC) Oral squamous cell carcinoma
(circRNAs) Circular RNAs
(FTO) Fat mass and obesity-associated protein
(m6A) N6-methyladenosine
(qRT-PCR) Quantitative real-time PCR
(PBS) Phosphate Buffered Saline
(RIP) RNA Immunoprecipitation
(RIPA) Radio Immunoprecipitation Assay Lysis buffer,
(SDS-PAGE) Sodium dodecyl sulfate-polyacrylamide gel electrophoresis
(ECL) Electrochemiluminescent
(CHX) Cycloheximide
(ROC) Receiver operating characteristic
(NEAT1) Nuclear paraspeckle assembly transcript 1
(RBPs) RNA-binding proteins
(GDI2) GDP dissociation inhibitor 2
(mRNA) Messenger RNA
(HOK) Human oral keratinocyte
(ATCC) American Type Culture Collection
(DMEM) Dulbecco's modified Eagle's medium
(FBS) Foetal bovine serum
(FISH) Fluorescence in situ hybridization

Appendix A. Supplementary data

Supplementary data to this article can be found online at https://doi.org/10.1016/j.ncrna.2024.08.001.

References

[1] H. Sung, J. Ferlay, R.L. Siegel, M. Laversanne, I. Soerjomataram, A. Jemal, et al., Global cancer statistics 2020: GLOBOCAN estimates of incidence and mortality worldwide for 36 cancers in 185 countries, CA A Cancer J. Clin. 71 (3) (2021) 209–249.
[2] A. Chamoli, A.S. Gosavi, U.P. Shirwadkar, K.V. Wangdale, S.K. Behera, N. K. Kurrey, et al., Overview of oral cavity squamous cell carcinoma: risk factors, mechanisms, and diagnostics, Oral Oncol. 121 (2021 Oct) 105451.
[3] K. Nemeth, R. Bayraktar, M. Ferracin, G.A. Calin, Non-coding RNAs in disease: from mechanisms to therapeutics, Nat. Rev. Genet. 25 (3) (2024 Mar) 211–232.
[4] Z. Yang, L. Xie, L. Han, X. Qu, Y. Yang, Y. Zhang, et al., Circular RNAs: regulators of cancer-related signaling pathways and potential diagnostic biomarkers for human cancers, Theranostics 7 (12) (2017) 3106–3117.
[5] L.S. Kristensen, T. Jakobsen, H. Hager, J. Kjems, The emerging roles of circRNAs in cancer and oncology, Nat. Rev. Clin. Oncol. 19 (3) (2022 Mar) 188–206.
[6] C.Y. Yu, T.C. Li, Y.Y. Wu, C.H. Yeh, W. Chiang, C.Y. Chuang, et al., The circular RNA circBIRC6 participates in the molecular circuitry controlling human pluripotency, Nat. Commun. 8 (1) (2017 Oct 27) 1149.
[7] X. Gu, X. Li, Y. Jin, Z. Zhang, M. Li, D. Liu, et al., CDR1as regulated by hnRNPM maintains stemness of periodontal ligament stem cells via miR-7/KLF4, J. Cell Mol. Med. 25 (9) (2021 May) 4501–4515.
[8] J. Chen, B. Rao, Z. Huang, C. Xie, Y. Yu, B. Yang, et al., Circular RNA hsa_circ_0050386 suppresses non-small cell lung cancer progression via regulating the SRSF3/FN1 axis, J. Transl. Med. 22 (1) (2024 Jan) 47.
[9] W. Wei, K. Liu, X. Huang, S. Tian, H. Wang, C. Zhang, et al., EIF4A3-mediated biogenesis of circSTX6 promotes bladder cancer metastasis and cisplatin resistance, J Exp Clin Cancer Res CR 43 (1) (2024 Jan 2) 2.
[10] L. Meng, Y. Zhang, P. Wu, D. Li, Y. Lu, P. Shen, et al., CircSTX6 promotes pancreatic ductal adenocarcinoma progression by sponging miR-449b-5p and interacting with CUL2, Mol. Cancer 21 (1) (2022 Jun 1) 121.
[11] J. Lu, J. Ru, Y. Chen, Z. Ling, H. Liu, Ding, et al., N6 -methyladenosine-modified circSTX6 promotes hepatocellular carcinoma progression by regulating the HNRNPD/ATF3 axis and encoding a 144 amino acid polypeptide, Clin. Transl. Med. 13 (10) (2023 Oct).

[12] M. Zhu, D. Chen, C. Ruan, P. Yang, J. Zhu, R. Zhang, et al., High-throughput microarray reveals the epitranscriptome-wide landscape of m6A-modified circRNA in oral squamous cell carcinoma, Int. J. Mol. Sci. 24 (18) (2023 Sep 17) 14194.
[13] Z. Yang, W. Chen, Y. Wang, M. Qin, Y. Ji, CircKRT1 drives tumor progression and immune evasion in oral squamous cell carcinoma by sponging miR-495-3p to regulate PDL1 expression, Cell Biol. Int. 45 (7) (2021) 1423–1435.
[14] J. Yan, H. Xu, Regulation of transforming growth factor-beta 1 by circANKS1B/miR-515-5p affects the metastatic potential and cisplatin resistance in oral squamous cell carcinoma, Bioengineered 12 (2) (2021 Dec) 12420–12430.
[15] L. Yang, J. Ying, Q. Tao, Q. Zhang, RNA N6-methyladenosine modifications in urological cancers: from mechanism to application, Nat. Rev. Urol. (2024 Feb 12) 460–476.
[16] G. Zhang, J. Hou, C. Mei, X. Wang, Y. Wang, K. Wang, Effect of circular RNAs and N6-methyladenosine (m6A) modification on cancer biology, Biomed. Pharmacother. 159 (2023 Mar) 114260.
[17] H. Huang, Y. Wang, M. Kandpal, G. Zhao, H. Cardenas, Y. Ji, et al., FTO-dependent N 6-methyladenosine modifications inhibit ovarian cancer stem cell self-renewal by blocking cAMP signaling, Cancer Res. 80 (16) (2020 Aug 15) 3200–3214.
[18] X. Deng, R. Su, S. Stanford, J. Chen, Critical enzymatic functions of FTO in obesity and cancer, Front. Endocrinol. 9 (2018).
[19] C. Zhuang, C. Zhuang, X. Luo, X. Huang, L. Yao, J. Li, et al., N6-methyladenosine demethylase FTO suppresses clear cell renal cell carcinoma through a novel FTO-PGC-1α signalling axis, J. Cell Mol. Med. 23 (3) (2019 Mar) 2163–2173.
[20] W. Yi, Y. Yu, Y. Li, J. Yang, S. Gao, L. Xu, The tumor-suppressive effects of alpha-ketoglutarate-dependent dioxygenase FTO via N6-methyladenosine RNA methylation on bladder cancer patients, Bioengineered 12 (1) (2021 Dec) 5323–5333.
[21] Y. Li, R. Su, X. Deng, Y. Chen, J. Chen, FTO in cancer: functions, molecular mechanisms, and therapeutic implications, Trends Cancer 8 (7) (2022 Jul) 598–614.
[22] Z. Chen, J. Song, L. Xie, G. Xu, C. Zheng, X. Xia, et al., N6-methyladenosine hypomethylation of circGPATCH2L regulates DNA damage and apoptosis through TRIM28 in intervertebral disc degeneration, Cell Death Differ. 30 (8) (2023 Aug) 1957–1972.
[23] T. Schneider-Poetsch, J. Ju, D.E. Eyler, Y. Dang, S. Bhat, W.C. Merrick, et al., Inhibition of eukaryotic translation elongation by Cycloheximide and lactimidomycin, Nat. Chem. Biol. 6 (3) (2010 Mar) 209–217.
[24] W hai Fan, Y. Hou, F kai Meng, Wang X. fei, Luo Y. nan, Ge P. fei, Proteasome inhibitor MG-132 induces C6 glioma cell apoptosis via oxidative stress, Acta Pharmacol. Sin. 32 (5) (2011 May) 619–625.
[25] A. Radaic, P. Kamarajan, A. Cho, S. Wang, G.C. Hung, F. Najarzadegan, et al., Biological biomarkers of oral cancer, Periodontol 2023 (2000 Dec 10) 1–31.
[26] A. Miranda-Filho, F. Bray, Global patterns and trends in cancers of the lip, tongue and mouth, Oral Oncol. 102 (2020 Mar) 104551.
[27] E. Tahmasebi, M. Alikhani, A. Yazdanian, M. Yazdanian, H. Tebyanian, A. Seifalian, The current markers of cancer stem cell in oral cancers, Life Sci. 249 (2020 May 15) 117483.
[28] S. Wang, W. Li, L. Yang, J. Yuan, L. Wang, N. Li, et al., CircPVT1 facilitates the progression of oral squamous cell carcinoma by regulating miR-143-3p/SLC7A11 axis through MAPK signaling pathway, Funct. Integr. Genomics 22 (5) (2022 Oct) 891–903.
[29] J. Wang, S. Ouyang, S. Zhao, X. Zhang, M. Cheng, X. Fan, et al., SP1-Mediated upregulation of circFAM126A promotes proliferation and epithelial-mesenchymal transition of oral squamous cell carcinoma via regulation of RAB41, Front. Oncol. 12 (2022) 715534.
[30] W. Zhao, Y. Cui, L. Liu, X. Qi, J. Liu, S. Ma, et al., Splicing factor derived circular RNA circUHRF1 accelerates oral squamous cell carcinoma tumorigenesis via feedback loop, Cell Death Differ. 27 (3) (2020 Mar) 919–933.
[31] Y. Chen, Z. Li, J. Liang, J. Liu, J. Hao, Q. Wan, et al., CircRNA has_circ_0069313 induced OSCC immunity escape by miR-325-3p-Foxp3 axes in both OSCC cells and Treg cells, Aging 14 (10) (2022 May 16) 4376–4389.
[32] J. Jing, L. Song, D. Zuo, W. Li, Y. Sun, X. Ma, et al., Transcriptome expression profiles associated with diabetic nephropathy development, Mol. Cell. Biochem. 477 (7) (2022 Jul) 1931–1946.
[33] L. Zhang, H. Zhou, J. Li, X. Wang, X. Zhang, T. Shi, et al., Comprehensive characterization of circular RNAs in neuroblastoma cell lines, Technol. Cancer Res. Treat. 19 (2020) 1533033820957622.
[34] J. Li, D. Sun, W. Pu, J. Wang, Circular RNAs in cancer: Biogenesis, function, and clinical significance, Trends Cancer 6 (4) (2020 Apr) 319–336.
[35] X. Wang, R. Ma, X. Zhang, L. Cui, Y. Ding, W. Shi, et al., Crosstalk between N6-methyladenosine modification and circular RNAs: current understanding and future directions, Mol. Cancer 20 (1) (2021 Sep 24) 121.
[36] C. Chen, W. Yuan, Q. Zhou, B. Shao, Y. Guo, W. Wang, et al., N6-methyladenosine-induced circ 1662 promotes metastasis of colorectal cancer by accelerating YAP1 nuclear localization, Theranostics 11 (9) (2021) 4298–4315.
[37] X. Li, G. Tian, J. Wu, Novel circGFRα1 promotes self-renewal of female germline stem cells mediated by m6A writer METTL14, Front. Cell Dev. Biol. 9 (2021) 640402.
[38] Y.G. Chen, R. Chen, S. Ahmad, R. Verma, S.P. Kasturi, L. Amaya, et al., N6-Methyladenosine modification controls circular RNA immunity, Mol. Cell 76 (1) (2019 Oct 3) 96–109.e9.
[39] F. Wang, Y. Liao, M. Zhang, Y. Zhu, W. Wang, H. Cai, et al., N6-methyladenosine demethyltransferase FTO-mediated autophagy in malignant development of oral squamous cell carcinoma, Oncogene 40 (22) (2021 Jun) 3885–3898.
[40] D.Q. Li, C.C. Huang, G. Zhang, L.L. Zhou, FTO demethylates YAP mRNA promoting oral squamous cell carcinoma tumorigenesis, Neoplasma 69 (1) (2022 Jan) 71–79.
[41] X. Li, W. Chen, Y. Gao, J. Song, Y. Gu, J. Zhang, et al., Fat mass and obesity-associated protein regulates arecoline-exposed oral cancer immune response through programmed cell death-ligand 1, Cancer Sci. 113 (9) (2022 Sep) 2962–2973.
[42] H. Xia, Y. Wu, J. Zhao, C. Cheng, J. Lin, Y. Yang, et al., N6-Methyladenosine-modified circSAV1 triggers ferroptosis in COPD through recruiting YTHDF1 to facilitate the translation of IREB2, Cell Death Differ. 30 (5) (2023 May) 1293–1304.
[43] Y. Cui, Y. Wu, C. Wang, Z. Wang, Y. Li, Z. Jiang, et al., Isoliquiritigenin inhibits non-small cell lung cancer progression via m6A/IGF2BP3-dependent TWIST1 mRNA stabilization, Phytomedicine Int J Phytother Phytopharm. 104 (2022 Sep) 154299.
[44] T. Zhu, X.L.H. Yong, D. Xia, J. Widagdo, V. Anggono, Ubiquitination regulates the proteasomal degradation and nuclear translocation of the fat mass and obesity-associated (FTO) protein, J. Mol. Biol. 430 (3) (2018 Feb 2) 363–371.
[45] D.Y. Ruan, T. Li, Y.N. Wang, Q. Meng, Y. Li, K. Yu, et al., FTO downregulation mediated by hypoxia facilitates colorectal cancer metastasis, Oncogene 40 (33) (2021 Aug) 5168–5181.
[46] J. Jeschke, E. Collignon, C. Al Wardi, M. Krayem, M. Bizet, Y. Jia, et al., Downregulation of the FTO m6A RNA demethylase promotes EMT-mediated progression of epithelial tumors and sensitivity to Wnt inhibitors, Nat. Can. (Ott.) 2 (6) (2021 Jun) 611–628.
[47] R. Saikishore, P. Velmurugan, D. Ranjithkumar, R. Latha, T. Sathiamoorthi, A. Arun, et al., The circular RNA-miRNA Axis: a special RNA signature regulatory transcriptome as a potential biomarker for OSCC, Mol. Ther. Nucleic Acids 22 (2020 Dec 4) 352–361.
[48] Y. Cui, J. Liu, L. Liu, X. Ma, Y. Gui, H. Liu, et al., m6A-modified circFOXK2 targets GLUT1 to accelerate oral squamous cell carcinoma aerobic glycolysis, Cancer Gene Ther. 30 (1) (2023 Jan) 163–171.